PHYSICAL REVIEW A **79**, 052705 (2009)

Differential and integral cross sections for elastic electron scattering from CF_2

J. R. Francis-Staite, T. M. Maddern, and M. J. Brunger
ARC Centre for Antimatter-Matter Studies, SoCPES, Flinders University, GPO Box 2100, Adelaide 5001, Australia

S. J. Buckman
ARC Centre for Antimatter-Matter Studies, RSPhysSE, Australian National University, Canberra 0200, Australia

C. Winstead and V. McKoy
A. A. Noyes Laboratory of Chemical Physics, California Institute of Technology, Pasadena, California 91125, USA

M. A. Bolorizadeh
Department of Physics, Kerman University of Technology for Graduate Studies, Mahan, Iran

H. Cho
Department of Physics, Chungnam National University, Daejeon, Republic of Korea

(Received 2 April 2009; published 18 May 2009)

We report the results of measurements and calculations of differential and integral cross sections for elastic electron scattering from the CF_2 molecular radical. The energy range of the present investigation was 2–20 eV, while the angular distributions were measured at specific angles within the scattered electron range $20°-135°$. The calculations employed the Schwinger multichannel method and were carried out both in the static-exchange and static-exchange plus polarization (SEP) approximations, with generally quite good agreement found between the data and the SEP level results. This was particularly true at lower energies, illustrating the importance of correctly accounting for the polarization in these collisions.

DOI: 10.1103/PhysRevA.79.052705 PACS number(s): 34.80.Bm

I. INTRODUCTION

The important role that molecular radicals play in a range of electron-driven processes, including radiation damage in tissue, gas discharges, low-temperature plasma etch environments, and deposition technologies, is now well established [1]. In particular fluorocarbon feedstock gases are regularly employed as etching gases in a range of applications, ultimately leading through electron-impact dissociation to the production of CF_X ($X=1,2,3$) radicals which are responsible for several important chemical and physical processes on substrates. Modeling of the processes in these plasma reactors relies on a range of data inputs including absolute electron collision rates and cross sections for the relevant plasma species [2].

In this paper we extend our earlier work [3], which treated elastic electron scattering from CF_2 in the energy range 30–50 eV, to lower energies. Apart from this previous report from our group, absolute cross-section measurements for e^--CF_2 scattering are limited to partial [4] and total [5] ionization cross sections, measured using a fast-neutral-beam technique. Total CF_2 ionization cross sections have been estimated using a modified binary-encounter-dipole method [4] and total scattering and ionization cross sections by a complex scaling potential technique [6]. Integral elastic and excitation cross sections for e^--CF_2 scattering have been computed using an R-matrix approach [7], as have differential cross sections (DCSs) for elastic scattering [8], while differential and integral cross sections for elastic scattering have also been calculated using the iterative Schwinger variational method (ISVM) combined with the distorted-wave (DW) approximation [9]. Finally, we note our original Schwinger multichannel (SMC) [3] calculations. Those results, when compared against our measured differential and integral cross-section data between 30 and 50 eV, gave good agreement at the static-exchange (SE) level. It is nonetheless clear that available experimental and theoretical studies for electron scattering from the CF_2 radical remain limited, with a desire to somewhat improve this situation as one of the motivations behind this study.

The structure for the remainder of this paper is as follows. In Sec. II we briefly describe our experimental apparatus and measurement techniques, while in Sec. III details of our computations are provided. Thereafter our results and a discussion of those results are presented. Where possible, comparison to cross sections calculated using other theoretical models will be made. Finally, some conclusions from the present work will be drawn.

II. EXPERIMENTAL APPARATUS AND METHODOLOGY

The apparatus and procedures used to perform the CF_2 cross-section measurements have been comprehensively described in some recent publications [10,11], and we do not need to repeat those details again here. Briefly, the experiment is a crossed-beam electron-scattering experiment comprising four differentially pumped chambers. The first chamber contains a solenoid valve, a pyrolytic nozzle, and a skimmer and is pumped on by a 10″ diffusion pump. The second chamber, separated from the first by a skimmer, houses ten fixed-angle electron detectors, spanning an angular range $-45°-135°$, and is pumped on by a 156 1/s turbomolecular pump. The third chamber contains the electron

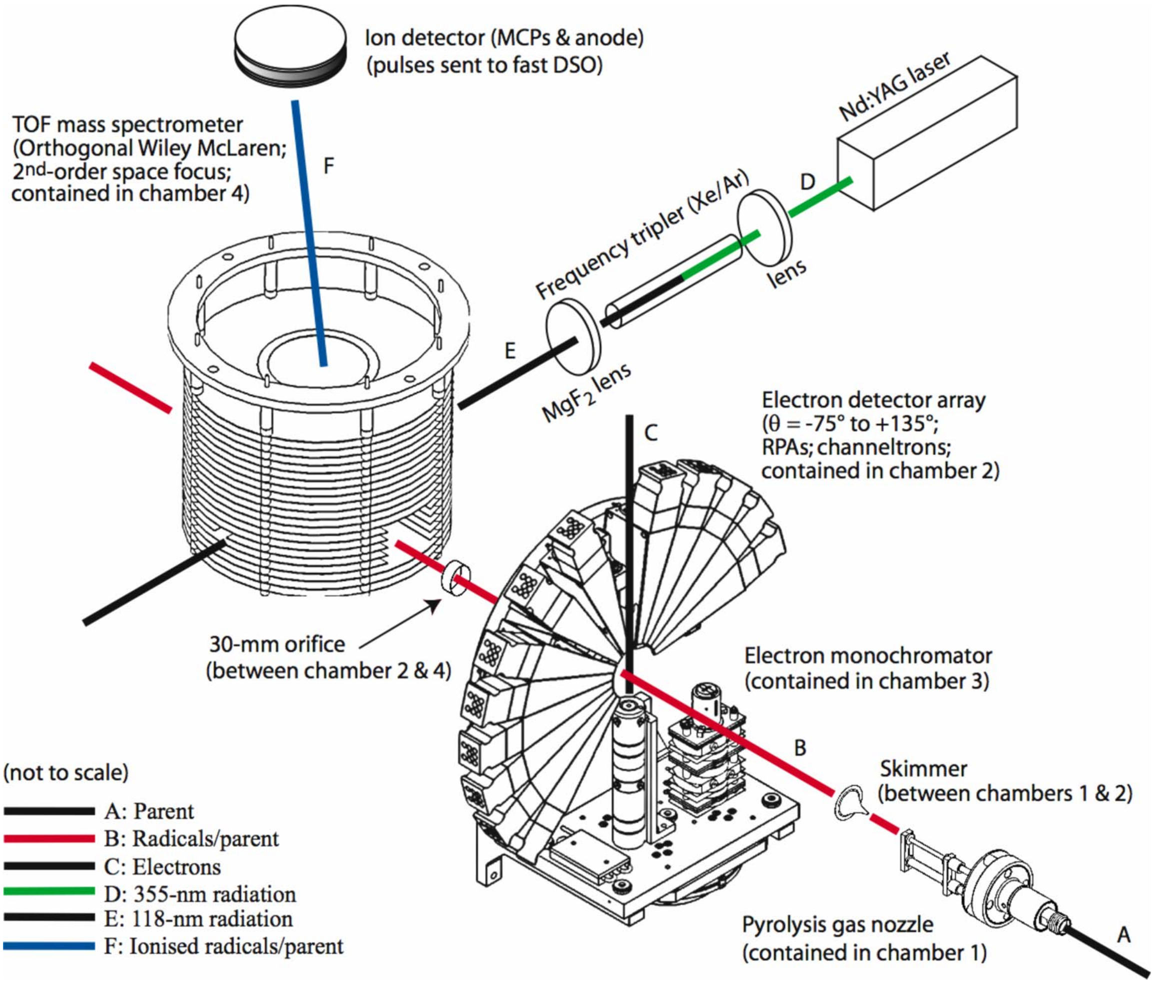

FIG. 1. (Color online) A schematic of the present experimental configuration.

monochromator and is differentially pumped by a 50 1/s turbomolecular pump. The fourth and final chamber, separated from the second by a 30 mm aperture, houses a time-of-flight mass spectrometer (TOFMS), which monitors the molecular-beam composition in conjunction with 118 nm radiation used to single-photon ionize species, and is evacuated by a 6″ diffusion pump. A schematic for this experimental layout is shown in Fig. 1.

Following pyrolysis of the parent C_2F_4 molecules, the heated products in the beam undergo cooling through supersonic expansion. A skimmer, placed downstream from the pyrolytic nozzle, serves to collimate the radical beam for passage through to the scattering chamber. For flash pyrolysis of pure C_2F_4 at 1188 °C the resultant supersonic expansion consists almost exclusively (>99%) of CF_2 radicals [3]. With the pyrolysis tube at room temperature, a strong C_2F_4 peak was observed in the TOFMS. When the pyrolysis temperature was now raised to 855 °C the C_2F_4 TOFMS peak began to decline, indicating the onset of pyrolysis, a result consistent with the previous work [12]. As the pyrolysis temperature was further increased, the C_2F_4 signal further diminished until it vanished at 1188 °C. This temperature represents that at which C_2F_4 is fully pyrolized, and it is also where all our measurements were conducted. Note that the temperature of the pyrolysis nozzle was measured with an optical pyrometer. A previous study [12] also measured the full pyrolysis of C_2F_4 at this temperature and found CF_2 to be the predominant (>99%) product.

The electron monochromator incorporates a thoriated tungsten filament, in a Pierce configuration element, which emits electrons through thermionic emission. Those electrons are focused into a hemispherical selector by two three-element aperture-type lenses and then guided into the scattering region by two cylindrical lens stages. Collimating apertures and electrostatic deflectors are incorporated throughout the monochromator to ensure optimum performance. The electron monochromator therefore produces a well-collimated well-focused monoenergetic electron beam which is scattered from the molecular beam. In the present work cross sections were measured at 13 electron energies (2, 3, 4, 5, 6, 8, 10, 12, 14, 15, 16, 18, and 20 eV). Such a fine energy grid is unusual in most scattering experiments but was undertaken here both to provide a comprehensive test for the computations and to search for resonances predicted in the elastic channel by those calculations [3,8,9].

Electrons scattered from the molecular target beam are detected by an array of rectangular section channeltrons (Sjuts KBL210), each preceded by a retarding potential analyzer (RPA), consisting of ten lens elements and a deflector, to filter out electrons not scattered elastically. Each channeltron-RPA detector is shielded from the scattering region in a grounded, wedge-shaped housing with each detector opening originally subtending a solid angle of 0.003 sr with respect to the scattering center. There were ten fixed-angle positions employed for the detectors in this study of −45°, −30°, 20°, 40°, 60°, 75°, 90°, 105°, 120°, and 135°, with this configuration being adopted because it effectively enabled a DCS to be simultaneously measured at each energy.

The absolute cross-section scale is set by a relatively new procedure [10] known as the pressure-rise skimmed supersonic relative density (p-SSRDM) method. Here the elastic DCS (σ) of the unknown (U) species is given in terms of that of a reference (R) species by [10]

$$\sigma_{\mathrm{U}} = \sigma_{\mathrm{R}} \left(\frac{\Delta P_d^* S_p}{Q v_\infty \dot{N}_e} \right)_{\mathrm{R}} \left(\frac{Q v_\infty \dot{N}_e}{\Delta P_d^* S_p} \right)_{\mathrm{U}}, \tag{1}$$

where ΔP_d^* is the corrected measured pressure-rise reading, Q is the total ionization cross section for the species of interest at 150 eV (see, e.g., [4]), v_∞ is the terminal velocity of the ideal-gas molecules in a skimmed supersonic expansion, S_p are the pumping speeds, and $\dot{N}_e$ is the measured elastic count rate. The reference species chosen to normalize the CF_2 cross sections was CF_4 because this molecule does not undergo flash pyrolysis at 1188 °C and also because an extensive set of accurate and reliable elastic DCS already exists for it in the literature [13]. Note that to check the validity of the earlier CF_4 data, which were taken at room temperature, a series of elastic DCS measurements for electron scattering from "hot" CF_4 were also made with the present apparatus. The level of agreement between those measurements and the room-temperature data was excellent, so that we have confidence in using the room-temperature CF_4 cross sections [13] as our reference. As CF_2 has a tendency to adhere to chamber walls, pumping speeds for CF_2 and CF_4 were explicitly measured rather than calculated in terms of the molecular mass. The chamber pressure P is related to the pumping speed S_p and elapsed time t by

$$P(t) = P_i e^{-tS_p/V}, \tag{2}$$

where V is the chamber volume and P_i is the initial pressure when the pulsed nozzle was shut off. The chamber pressure was logged as a function of time immediately after shut off and then the ratio of the pumping speeds determined via Eq. (2) as input to the p-SSRDM normalization.

A complete description of the uncertainties associated with our p-SSRDM measurements was given by Hargreaves *et al.* [10]. Briefly, uncertainties are taken as the quadrature sum of the statistical errors (2%–10%), uncertainty in the pressure rise (5% each), uncertainty in the calibrated pumping speeds (10%), uncertainty in the ionization cross sections (2%–25%), and the uncertainty in the CF_4 DCS (~20%). The total uncertainty in the present CF_2 DCSs is therefore typically in the range 30%–60%.

III. CALCULATIONS

The SMC method and its implementation for parallel computers have been described elsewhere [14–17], so we give here only the details specific to the present calculations. We assumed C_{2v} point-group symmetry for the CF_2 molecule and optimized the nuclear geometry at the level of second-order Möller-Plesset perturbation theory in the 6−31G(d) basis set as contained in the electronic structure package GAMESS [18], leading to a C-F bond distance of 1.3145 Å and an F-C-F bond angle of 104.196°. Electron-scattering calculations were carried out using the SMC method both in the SE approximation, i.e., with polarization neglected, and in the static-exchange plus polarization (SEP) approximation. Both the SE and SEP calculations were carried out in the 6–311G basis set as contained in GAMESS together with a $1s1p3d$ set of supplementary functions, for which the default exponents and splitting factors of GAMESS were used. The $x^2+y^2+z^2$ linear combinations of the Cartesian d orbitals were omitted. In the SE calculations, the variational space included only doublet configuration state functions (CSFs) formed by antisymmetrizing the Hartree-Fock ground state with each empty (virtual) molecular orbital. The SEP calculation included, in addition, a closed-channel space comprising doublet CSFs with a single vacancy in one of the occupied valence orbitals and two electrons in virtual orbitals. To obtain a compact description of the closed-channel space [19], the virtual orbitals were transformed to modified virtual orbitals (MVOs) [20] using a 6^+ cationic Fock operator, and we included all singlet-coupled excitations from the nine valence orbitals into the 30 lowest-energy MVOs. Such singlet-coupled virtual excitations capture the relaxation of the target charge density that corresponds to the classical idea of polarization. However, in molecules that possess low-lying triplet excited states, it is also important to include virtual (or real) excitations to those triplet states in the scattering calculation. The ${}^3B_1$ state of CF_2 lies only 2.3 eV above the ${}^1A_1$ ground state [21], and we have accordingly included the triplet-coupled excitation from the highest occupied orbital ($6a_1$) of the ground state into the lowest MVO ($2b_1$) in forming our closed-channel space. The resulting configuration space contained 5014 CSFs in ${}^2A_1$ symmetry, 4459 in ${}^2A_2$, 4490 in ${}^2B_1$, and 4969 in ${}^2B_2$ symmetry.

IV. RESULTS AND DISCUSSION

In Table I we present our experimental absolute elastic differential cross sections for electron scattering from the CF_2 molecular radical. Also included in this table are the absolute errors on our measured data and, for energies 30 eV and above, the earlier results from Maddern *et al.* [3] and a 25 eV result by Maddern *et al.* [11]. A representative selection of these data are plotted in Figs. 2(a)–2(d), along with the results from our Schwinger multichannel calculations at the SE and SEP levels and, where possible, results from earlier R-matrix [8] and ISVM-DW [9] computations. In our original study of the e^-+CF_2 system [3], we concluded that our SMC calculations at the SE level provided a good description of this scattering system for incident electron energies between 30 and 50 eV. In this investigation we find that this observation (see Fig. 2) continues to hold true down to energies around 10 eV. Below 10 eV the importance of appropriately accounting for polarization becomes increasingly

TABLE I. Experimental elastic differential cross sections of CF_2 for electron-impact energies from 2 to 50 eV in units of 10^{-16} cm^2 sr^{-1}. Untabulated previously published [3,11] data are also included here for completeness.

Energy	Scattering angle									
(eV)	20°	30°	40°	45°	60°	75°	90°	105°	120°	135°
2.00					0.28 ± 0.27	0.14 ± 0.17				
3.00			1.35 ± 0.45		0.93 ± 0.31	0.77 ± 0.25	0.62 ± 0.20	0.54 ± 0.18		
4.00			1.26 ± 0.41		1.12 ± 0.37	0.80 ± 0.26	0.46 ± 0.15	0.58 ± 0.19	0.88 ± 0.29	
5.00	2.04 ± 0.81		1.19 ± 0.39		0.98 ± 0.32	0.63 ± 0.21	0.42 ± 0.14	0.51 ± 0.17	0.33 ± 0.11	
6.00			1.56 ± 0.41		1.03 ± 0.22	0.75 ± 0.16	0.42 ± 0.08	0.43 ± 0.09	0.36 ± 0.11	
8.00			1.47 ± 0.41		0.58 ± 0.17	0.40 ± 0.15	0.22 ± 0.08	0.29 ± 0.12	0.35 ± 0.16	
10.00		1.79 ± 0.48	1.66 ± 0.44		0.84 ± 0.33	0.53 ± 0.20	0.46 ± 0.14	0.40 ± 0.13	0.34 ± 0.11	0.45 ± 0.15
12.00		3.19 ± 0.88	1.86 ± 0.50		0.67 ± 0.29	0.66 ± 0.24	0.49 ± 0.15	0.46 ± 0.15	0.31 ± 0.11	0.51 ± 0.16
14.00		2.08 ± 0.92	2.00 ± 0.59				0.53 ± 0.19	0.57 ± 0.27	0.38 ± 0.16	0.46 ± 0.21
15.00			1.79 ± 0.99	0.93 ± 0.34			0.438 ± 0.13	0.63 ± 0.32	0.44 ± 0.22	
16.00		2.59 ± 0.76	1.72 ± 0.46		0.74 ± 0.33	0.68 ± 0.26	0.54 ± 0.16	0.58 ± 0.19	0.52 ± 0.18	0.68 ± 0.23
18.00			1.07 ± 0.29		0.77 ± 0.30	0.29 ± 0.11	0.29 ± 0.09	0.31 ± 0.10	0.21 ± 0.07	0.36 ± 0.12
20.00			0.73 ± 0.24		0.34 ± 0.11	0.30 ± 0.10	0.22 ± 0.07	0.19 ± 0.06	0.24 ± 0.08	0.48 ± 0.16
25.00			0.75 ± 0.26		0.39 ± 0.15	0.20 ± 0.08	0.16 ± 0.06	0.15 ± 0.07	0.20 ± 0.10	0.54 ± 0.21
30.00	4.27 ± 1.73		0.66 ± 0.22		0.35 ± 0.13	0.23 ± 0.09	0.11 ± 0.04	0.08 ± 0.04	0.20 ± 0.09	0.38 ± 0.14
40.00	4.87 ± 1.46		0.60 ± 0.18		0.38 ± 0.11	0.28 ± 0.08	0.12 ± 0.04	0.08 ± 0.03	0.15 ± 0.05	0.38 ± 0.12
50.00	3.70 ± 1.01		0.34 ± 0.09		0.22 ± 0.06	0.13 ± 0.03	0.06 ± 0.02	0.06 ± 0.02	0.11 ± 0.03	0.46 ± 0.14

apparent, as can be seen explicitly in Figs. 2(a) and 2(b) at 3 and 6 eV incident electron energy, respectively. This is perhaps not surprising given that CF_2 has a significant dipole polarizability ($12.4a_0^3$ [22]) compared with water, another small triatomic having C_{2v} symmetry ($9.67a_0^3$ [23]), and given also that the permanent dipole moment of CF_2 is quite modest (0.469 D [24] vs 1.854 D for water [25]). In general we would characterize the overall level of agreement, over the common scattered electron angular range, between our SMC calculations and our measurements as very good. Agreement between the present data and earlier calculations [8,9] is less satisfactory but nonetheless fair. As seen in Fig. 2, the earlier calculations produce larger DCSs at forward angles than seen in the present measurements or SEP calculations. The Born correction included in the *R*-matrix and ISVM-DW results only becomes significant at angles below about 10° and thus cannot account for the discrepancy. Rather, we believe it indicates that the previous calculations do not sufficiently account for polarization effects. Note that, in Fig. 2, both the *R*-matrix and the ISVM-DW results are closer to our SE results than to our SEP results at forward angles. This conclusion is also consistent with the integral cross section (ICS) [see Fig. 3], as we discuss later.

The current measured angular distributions were limited to scattering angles of 20° and above, even though there is provision for a channeltron-RPA detector at 15°. This detector, particularly at the lower energies, regularly "saturated" due to a combination of the large field of view of our channeltron-RPA detectors and the relatively uncollimated nature of our molecular beam. While attempts were made to reduce the field of view of those RPAs by inserting smaller apertures into the forward-angle detectors, they were not entirely successful. Further collimation of our molecular beam was also considered, but was not pursued due to our concern that we would consequently "lose signal" at the larger scattering angles where the cross sections are smaller. This lack of forward-angle data was unfortunate [see Figs. 2(a) and 2(b)], as some of the major differences between the various theories occur at scattering angles less than 20°. In particular both the *R*-matrix [8] and ISVM-DW [9] calculations include an explicit Born-closure correction to account for the permanent dipole moment of CF_2, whereas the present SMC results do not.

In Table I, for incident electron energies of 14 and 15 eV, there is an unexpected omission in the measured DCS at scattering angles between 40° and 75° (in each case). The absence of CF_2 differential cross sections at these angles were not caused by any lack of CF_2 elastic signal; rather, these measurements coincided with a deep minimum in the 14 and 15 eV CF_4 elastic DCSs [13] so that in fact the problem in this case was a lack of CF_4 elastic signal.

Our data in Table I were extrapolated at each energy using a molecular phase-shift analysis (MPSA) procedure [26] to 0° and 180° before being integrated to derive ICS for e^--CF_2 scattering. We note that, at each energy, the fit to the measured DCS using our MPSA was excellent, and in almost all cases the extrapolations to 0° and 180° showed a strong resemblance to either our SMC-SE or SMC-SEP results. Nonetheless, we do appreciate that using the MPSA to extrapolate from ~20° to 0° and ~135° to 180° potentially does lead to some errors in our experimental ICS. The present experimental ICSs are listed in Table II and plotted in Fig. 3 along with our SMC results. We note that the uncertainties in our experimental ICS are typically ~45%, with this rather large error being mainly due to the uncertainties on our DCS and the uncertainties associated with the extrapolation of our

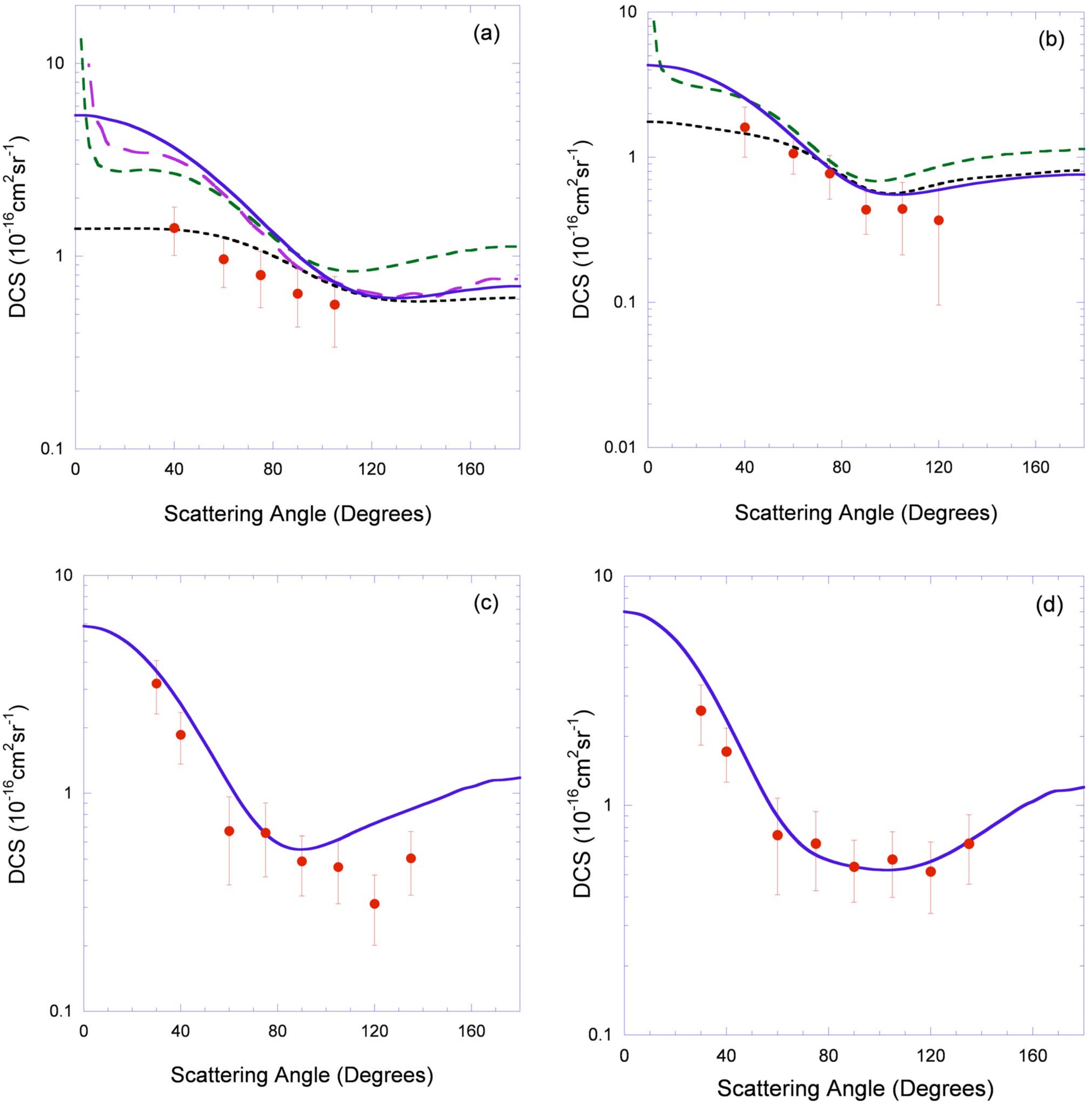

FIG. 2. (Color online) Absolute differential cross sections (10^{-16} cm^2 sr^{-1}) for elastic electron scattering from the CF_2 radical at (a) 3, (b) 6, (c) 12, and (d) 16 eV. The present data (●) and SEP (- - -) and SE (blue ———) level calculations are compared against the earlier computation results of Rozum and Tennyson [8] (purple —— ——) and Lee *et al.* [9] (green – –).

DCS at each energy. Also plotted in Fig. 3 are ICS from *R*-matrix computations [7] and the ISVM-DW [9] approach, as well as our earlier experimental data from Maddern *et al.* [3].

It is clear in Fig. 3 that the calculations predict a significant resonance enhancement of the elastic ICS at low energies, albeit with the energy of the resonance peak being different in each case. Specifically the current SMC-SEP calculation predicts the resonance peak to occur at an energy below ~0.1 eV (not shown), the SMC-SE calculation places the peak at ~2 eV, the *R*-matrix result is at ~1 eV, while that for the ISVM-DW method is at ~1.6 eV. Unfortunately, our present measurements do not extend to low enough energies to clarify these results. However, we note that because polarization is an attractive interaction, it shifts resonances to lower energies. Thus the fact that the *R*-matrix [7] and ISVM-DW [9] results put the main resonance peak at higher energies than our SEP calculation is consistent with those calculations including less polarization.

A stable CF_2^- anion exists, with an adiabatic electron affinity of 0.18 ± 0.02 eV determined by Schwartz *et al.* [21] using photodetachment spectroscopy. This anion has the same $^2B_1$ electronic configuration as the resonance under discussion. In other words, the resonance energy is the (nega-

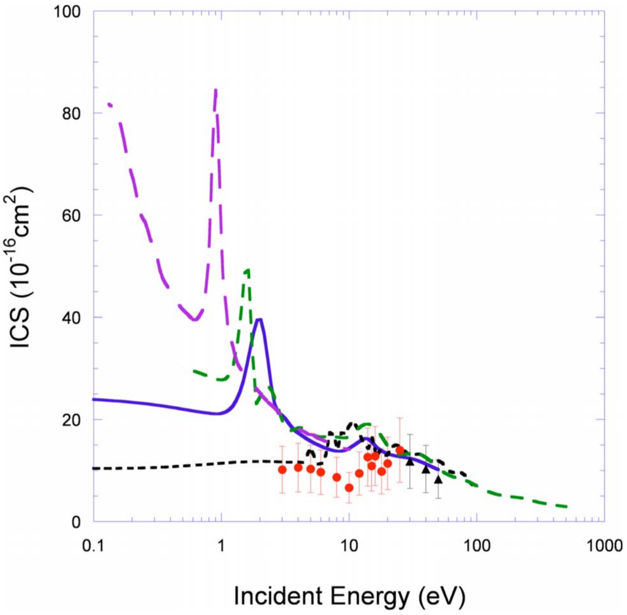

FIG. 3. (Color online) Absolute integral cross sections (10^{-16} cm^2) for elastic electron scattering from the CF_2 radical. The present data (●) and SEP (- - -) and SE (blue ——) level calculations are compared against the earlier computation results of Rozum *et al.* [7] (purple —— —— ——), Lee *et al.* [9] (green – –), and our own earlier data [3] (▲).

TABLE II. Experimental elastic integral cross sections of CF_2 for electron-impact energies from 3 to 50 eV. Untabulated previously published [3,11] data are also included here for completeness.

Energy (eV)	ICS[a] (10^{-16} cm^2)
3.00	10.20
4.00	10.60
5.00	10.33
6.00	9.69
8.00	8.70
10.00	6.64
12.00	9.45
14.00	12.66
15.00	10.91
16.00	12.84
18.00	9.85
20.00	11.40
25.00	14.00
30.00	11.80
40.00	10.30
50.00	8.30

[a] Uncertainties in ICS measurements are in the order of 45%.

tive) vertical electron affinity of the ground-state ion. In setting the resonance below 0.1 eV, our SEP calculation indicates that the anion is either very nearly bound or actually bound at the vertical geometry; given our neglect of vibrational motion, and given that errors of a few tenths of an eV are typical for this sort of calculation, we cannot be more definitive. On the other hand, the calculations that place the resonance higher, at 1–2 eV, predict that the anion energy rises quite a bit (from −0.18 to 1–2 eV) between the anion equilibrium geometry and that of the neutral species.

A second, much weaker, resonance feature occurs near 15 eV in the ICS from our SMC-SE calculation and that obtained in the ISVM-DW approach [9]. In our SE calculation, this feature arises from overlapping broad resonances, one in $^2A_1$ at about 12 eV and one in $^2B_2$ at about 13.5 eV, while Lee *et al.* [9] reported a $^2B_2$ resonance at about 15 eV. There does appear to be some experimental support for the existence of this structure, although the errors on our measured ICS preclude us from being more definitive here. We would characterize the level of agreement between the present measured ICS and our SMC calculation as being good, as might be anticipated from our previous discussion of the DCS. In particular we highlight that, at energies below 8 eV, only the SMC-SEP result agrees with the experimental ICS, even when the uncertainties on the current measurements are taken into account.

V. CONCLUSIONS

We have reported measurements and SMC calculations for elastic electron scattering from CF_2. Both differential and integral cross sections were presented between 2 and 20 eV, with generally good agreement found between our measurements and calculations. Such data are important for our quantitative understanding, through modeling [2], of how plasma reactors, in which CF_2 is one of the active constituents, function at the nanoscale. One of the highlights of the present study was the clear role played by polarization in the lower energy scattering regime of this system. Further experiments at energies less than 2 eV will be required to definitively test whether the theoretically predicted resonance exists and, if so, at what energy. Such experiments require a modification to our electron monochromator, which is currently under consideration.

ACKNOWLEDGMENTS

We thank the Australian Research Council for the financial support through their Centre of Excellence program. C.W. and V.M. acknowledge support from the Chemical Sciences, Geosciences and Biosciences Division, Office of Basic Energy Sciences, Office of Science, U.S. Department of Energy, and use of the resources of the Jet Propulsion Laboratory's Supercomputing and Visualization Facility. M.A.B. thanks Flinders University for the financial support that allowed his participation in this project, while H.C. acknowledges the Australian Academy of Science and the Korea Science and Engineering Foundation for their financial assistance in supporting his visit to Flinders University and the ANU. Finally, J.F.S. thanks the Australian government for financial support through the APA program.

[1] S. J. Buckman *et al.*, J. Phys.: Conf. Ser. **133**, 012001 (2008).

[2] National Research Council I, *Database Needs for Modelling and Simulation of Plasma Processing* (National Academy, New York, 1996).

[3] T. M. Maddern, L. R. Hargreaves, J. R. Francis-Staite, M. J. Brunger, S. J. Buckman, C. Winstead, and V. McKoy, Phys. Rev. Lett. **100**, 063202 (2008).

[4] W. M. Huo, V. Tarnovsky, and K. Becker, Chem. Phys. Lett. **358**, 328 (2002).

[5] V. Tarnovsky and K. Becker, J. Chem. Phys. **98**, 7868 (1993).

[6] B. K. Antony, K. N. Joshipura, and N. J. Mason, J. Phys. B **38**, 189 (2005).

[7] I. Rozum, N. J. Mason, and J. Tennyson, J. Phys. B **35**, 1583 (2002).

[8] I. Rozum and J. Tennyson, J. Phys. B **37**, 957 (2004).

[9] M. T. Lee, I. Iga, L. E. Machado, L. M. Brescansin, E. A. y Castro, and G. L. C. de Souza, Phys. Rev. A **74**, 052716 (2006).

[10] L. R. Hargreaves, J. R. Francis-Staite, T. M. Maddern, M. J. Brunger, and S. J. Buckman, Meas. Sci. Technol. **18**, 2783 (2007).

[11] T. M. Maddern, L. R. Hargreaves, M. Bolorizadeh, M. J. Brunger, and S. J. Buckman, Meas. Sci. Technol. **19**, 085801 (2008).

[12] M. R. Cameron and S. H. Kable, Rev. Sci. Instrum. **67**, 283 (1996).

[13] L. Boesten, H. Tanaka, A. Kobayashi, M. A. Dillon, and M. Kimura, J. Phys. B **25**, 1607 (1992).

[14] K. Takatsuka and V. McKoy, Phys. Rev. A **24**, 2473 (1981).

[15] K. Takatsuka and V. McKoy, Phys. Rev. A **30**, 1734 (1984).

[16] C. Winstead and V. McKoy, Adv. At., Mol., Opt. Phys. **36**, 183 (1996).

[17] C. Winstead and V. McKoy, Comput. Phys. Commun. **128**, 386 (2000).

[18] M. W. Schmidt *et al.*, J. Comput. Chem. **14**, 1347 (1993).

[19] C. Winstead, V. McKoy, and M. H. F. Bettega, Phys. Rev. A **72**, 042721 (2005).

[20] C. W. Bauschlicher, J. Chem. Phys. **72**, 880 (1980).

[21] R. L. Schwartz, G. E. Davico, T. M. Ramond, and W. C. Lineberger, J. Phys. Chem. A **103**, 8213 (1999).

[22] NIST Computational Chemistry Comparison and Benchmark Database, NIST Standard Reference Database 101, edited by R. D. Johnson III, 2005, http://srdata.nist.gov/cccbdb

[23] C. Millot and B. J. Costa Cabral, Chem. Phys. Lett. **460**, 466 (2008).

[24] W. H. Kirchhoff, D. R. Lide, Jr., and F. X. Powell, J. Mol. Spectrosc. **47**, 491 (1973).

[25] S. L. Shostak, W. L. Ebenstein, and J. S. Muenter, J. Chem. Phys. **94**, 5875 (1991).

[26] L. Campbell, M. J. Brunger, A. M. Nolan, L. J. Kelly, A. B. Wedding, J. Harrison, P. J. O. Teubner, D. C. Cartwright, and B. McLaughlin, J. Phys. B **34**, 1185 (2001).